JOURNAL OF COMPUTATIONAL PHYSICS 75, 359–383 (1988)

Random-Vortex Simulation of Transient Wall-Driven Flow in a Rectangular Enclosure

Y. CHOI, J. A. C. HUMPHREY, AND F. S. SHERMAN

Department of Mechanical Engineering, University of California, Berkeley, California 94720

Received August 21, 1986; revised March 20, 1987

Two-dimensional transient flow in square cavity, following impulsive acceleration of the sliding wall, is simulated by random-vortex calculations of the type initiated by A. Chorin. Comparison calculations are made using a transient finite-difference method that is first-order accurate in time and second-order accurate in space. The Reynolds number, R, based on the sliding wall length and speed, is 2000, 5000, or 10,000. The simulated history starts when the moving wall starts, ends when the wall has moved three times its length, and shows the development of primary and secondary eddies in the corner where the boundary layer on the moving wall is peeled off by the stationary wall. Special features of this random-vortex simulation include: (1) the use of the closed-form expression for the velocity induced by a line vortex in a rectangular enclosure; (2) special treatment of regions very close to the corners where the sheet-like elements, ordinarily used in a very thin wall layer, are inappropriate; and (3) the generation of a small (three-member) ensemble of simulations at each Reynolds number. Comparisons between the two numerical schemes were made at Reynolds numbers of 2000 and 5000. A comparison with experimental data of Koseff is given for $R = 2000$. Both numerical methods exhibited the same qualitative flow features and were in fair quantitaive agreement. The random-vortex calculations show somewhat better agreement with the laboratory experiment.

1. INTRODUCTION

Steady flow in a rectangular cavity, driven by the sliding motion of one of the walls, has become a paradigm of viscous flow; it has been extensively explored in the laboratory [1], and has been a standard target for numerical simulation [2–17]. The simple configuration of the boundary allows one to concentrate the resources of a particular numerical technique on the resolution of interesting detailed flow features, which appear in increasing number as the Reynolds number increases.

Relatively little attention has been paid to the transient flow, which would follow impulsive acceleration of the sliding wall, even though this idealized case seems to offer considerable intrinsic interest and some good challenges for numerical analysis. Unlike the steady flow, the starting flow will be irrotational within a large fraction of the rectangle, and the random-vortex simulation seems attractive because it may reveal a very interesting picture before the number of computational

0021-9991/88 $3.00

elements becomes unmanageably large. This picture certainly will include features which are hard to capture in a computation that employs a fixed Eulerian grid of any refinement, although it is possible that at very early times a local similarity solution, with a streamfunction of form $\psi = Urf(\xi, \theta)$, could be used to expand the scale of distance very near the troublesome corner. In this, r and θ are polar coordinates centered at the corner, U is the moving wall velocity and $\xi = r(4\nu t)^{-1/2}$ is the similarity variable. However, the analysis of the similarity solution could be a difficult task in itself, particularly in view of the velocity discontinuity imposed in the idealized problem at the end of the sliding wall.

Sharp corners present a special challenge to the random-vortex scheme as well, because the sheet-like elements, which are used to represent the vorticity distribution in a very thin region close to walls, are designed to mimic the behavior of vorticity in a boundary layer. This requires that an unambiguous outward normal vector exists at every point of the wall, and that the radius of curvature of the wall be very large compared to the distance from the wall to a sheet. External corners, as at the end of a splitter plate [18], and internal corners, as in the present problem, both cause difficulties which have not as yet been thoroughly resolved.

Nevertheless, random-vortex simulations are becoming popular, and in cases that do not crucially involve sharp corners, they have demonstrated both accuracy in the description of relatively bland steady flows [19], and impressively faithful descriptions of a wealth of small-scale detail in transiently separating flows [20–21]. Thus, the method seemed an obvious candidate for this problem.

One of the finite-difference algorithms which has been notably succesful in application to the steady flow limit of the present problem is the REBUFFS code [22–26]. Since we have accumulated experience with the use of this code on transient flows, it seemed interesting to run a comparison between its capabilities and those of the random-vortex method.

Finally, recent laboratory experiments by Koseff [1] provide information about the starting flow, at a Reynolds number of 2000, suitable as a standard of comparison for the two calculation schemes. In particular, the starting flow has been observed to be highly two-dimensional, even at values of Re which correspond to eventually turbulent flow. Presumably, the starting flow becomes unstable at some time, but the perturbations take a considerable time to grow, leaving an interesting period of flow development which should be well described by a theory of two-dimensional flow.

2. The Random-Vortex Method

The set of algorithms that has acquired the name *random-vortex method* was originally proposed by A. J. Chorin [27–29], and most subsequent analyses and applications of the method have been carried out by him, his colleagues, and students. However, there are important variants of the method, and potentially significant differences in detail, so that each author needs to explain the exact

procedure used to obtain a given result. What follows in this section is a very brief outline of the general method, and then a precise statement of the details built into the final random-vortex computer code used in this study.

2.1. *Synthesis of the Velocity Field*

The general method starts with the theorem for synthesis of a vector field, $\mathbf{u}(\mathbf{r}, t)$, given the fields of Δ and Ω, where $\Delta \equiv \operatorname{div} u$, and $\Omega \equiv \operatorname{curl} u$. This states that

$$\mathbf{u} = \mathbf{u}_v + \mathbf{u}_d + \mathbf{u}_p, \tag{1-1}$$

where $\mathbf{u}_v$, the *velocity due to vorticity*, may be computed by the Biot–Savart law, as though there were no solid boundaries; $\mathbf{u}_d$, the *velocity due to divergence*, is zero for strictly incompressible flow, as is assumed here; and $\mathbf{u}_p$ is the *velocity due to a solenoidal potential flow*, to be added so that the combined flow does not pass through solid walls and has, if appropriate, desired properties at infinity. Use of the Biot–Savart law ordinarily requires that the vorticity has compact support, or that it is distributed periodically in space.

2.2. *Computational Evaluation of the Biot–Savart Integral*

At any time after the start of the motion, the spatial distribution of vorticity is imitated by a set of spatially overlapping circular or linear elements, called blobs and sheets. Each element is characterized by a value of the circulation, which is assigned when the element is created, and held constant thereafter. Each element is further characterized by the velocity field which it induces at any point away from its center and is designed so that this velocity is always finite.

There is considerable flexibility available to the designer of such elements, and considerable evidence [30–31] that the design of the blobs can affect the accuracy with which the integral is approximated by the sum of contributions from a fixed number of blobs. We employed the original flat-topped blobs introduced by Chorin [27], and the sheets he introduced in [29]. These are the same elements used in [18–20]. Very recently, Tiemroth [21] has redone and extended the calculations of Cheer [20], using blobs of uniform vorticity and overlapping sheets with a tent-like distribution of strength along the sheet length. These modifications appear to make the method more robust, but were developed after the present calculations were completed. Figure 1 reminds us of the properties of the flat-

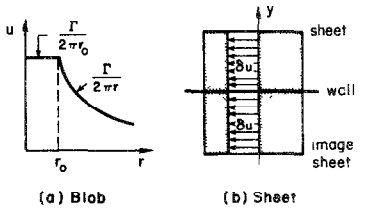

FIG. 1. Velocity fields associated with computational vorticity elements; δu is the velocity jump across the sheet.

topped blobs and the sheets. Note that each sheet is accompanied by an image, equally distant behind the wall, so that sheet plus image produce a uniform plug flow between them, and zero velocity elsewhere.

Ordinarily, the blob representation is used whenever the center of the element is farther than half a blob radius from the wall; the sheet representation is used elsewhere. In the present problem, the sheet representation is conceptually inappropriate very near the corners, and one of the corner regions is the seat of most of the interesting flow developments. This called for special treatment of the corner regions, specified below in Section 3.8.

The placement of the elements at a given time is determined by the equations of motion and the no-slip boundary condition, as will be described in Section 2.4.

2.3. *Generation of the Solenoidal Potential Flow*

The velocity induced by each vortex blob coincides, at points outside the blob, with the velocity induced by a line vortex of the same circulation. In [32], Choi and Humphrey present a closed-form solution, in terms of elliptic functions, that synthesizes $\mathbf{u}_v + \mathbf{u}_p$ for a single line vortex within a stationary rectangular enclosure; they also present a computationally economical algorithm for evaluation of the elliptic functions. For the present calculation, the closed-form expression for each element was modified by subtracting the $\mathbf{u}_v$ of a line vortex, and replacing it by the $\mathbf{u}_v$ of a blob.

The closed-form expression was obtained by summing the effects of an infinite array of image vortices, some of which are very close to the interior vortex if the latter lies very close to one or more walls. When interior line vortices are replaced by blobs, the images are also conceived to be blobs; thus a blob that is very close to a wall may overlap with one or two of its own closest image blobs, or with image blobs associated with neighboring interior elements. In this case, a further modification of the closed-form expression was made, to replace the overlapping images with blobs. The details are presented in Section 3.1.

Alternative procedures are also available to generate an approximation to $\mathbf{u}_p$. The simplest in concept would be an arithmetic summation of the contributions of a finite set of images, but it is shown in [32] that this is, for an adequate level of accuracy, computationally more expensive that the procedure followed here. A less expensive alternative employs fixed external arrays of singularities, such as line vortices, sources, sinks, or doublets, with strengths tuned at each time step so as to annul the flow through the wall at an equal number of collocation points. An excellent discussion and illustration of alternative techniques is given in [21].

2.4. *Time-splitting*

Another feature common to all versions of the random-vortex method is *sequential* simulation, during each increment of time, of the three physically simultaneous processes which affect the spatial distribution of vorticity. These processes are:

(1) *convection*, which is simulated by displacing vortex blobs or sheets with the local fluid velocity, keeping the circulation of each element constant;

(2) *generation*, which in the case of barotropic flow occurs only at the wall, in order to enforce the no-slip condition, and which is simulated by the introduction of new vortex elements at the wall; and

(3) *diffusion*, which is simulated by giving each element of vorticity an appropriate random displacement, drawn from a Gaussian distribution with zero mean and with variance proportional to $\nu \Delta t$, where ν is the fluid kinematic viscosity and Δt is the time increment in the numerical calculation. For a blob, independent displacements in x and y are drawn; a sheet is displaced only in the direction normal to the nearest wall.

There may be variety in the detailed implementation of each of these steps, but most workers use at least a second-order integrator for the convective displacement of vortex elements. We used Heun's improved Euler method [33] for blobs, but only a first-order Euler method for sheets. It has also been shown [34] that it is appropriate, with a second-order convective integrator, to split the diffusive displacement into two half steps, each drawn from a population of variance $\nu \Delta t$, but we followed [18, 20, 35] in using a single step from a population with variance $2\nu \Delta t$.

It is probably worth mentioning that we, and all the authors we imitated, observed a spontaneous misbehavior of the method, characterized by an oscillatory production of vortex elements of alternating sign, at locations where vorticity of only one sign is physically needed. Each author has struggled with this in a different way, as follows:

(1) Ellzey [18] let the *parasitic* elements, which seemed to have a physically unrealistic sign, be generated, but then weeded them out of the sheet layer by discarding pairs of elements of equal and opposite strength, when they met a proximity test.

(2) Ghoniem and Gagnon [19] reduced the percentage of parasitic elements by using more sheets, of smaller strength, to correct for a given slip velocity. They showed that this leads to a less than proportional increase of the total number of computational elements, because many of the elements in a crude simulation are parasites.

(3) Tiemroth [21], whose work followed ours, utilized tent-shaped sheets, designed to smooth the tangential variations of the sheet-induced flow, and used two half-steps for diffusion, together with a modified-Euler integrator for convection. This seemed to cure the problem, even when fairly strong sheets were formed.

Our own approach was simply to ignore a call for sheets of the wrong sign, along parts of the wall where the correct sign seemed obvious. The details are specified in Section 3.4. Given the results of Tiemroth, we would not use our technique again.

but it seems, like the equally arbitrary technique used by Ellzey, to have been harmless.

2.5. *Local Annihilation of Slip Velocity*

An intrinsic feature of the random-vortex method is a discretization of solid boundaries for the purpose of application of the no-slip condition. In the usual practice of the method, the slip velocity is annihilated by the introduction of new vortex elements, only at a discrete set of boundary points. These points may be distributed along the boundary in any desired way, but the correction that annihilates the slip at one of the collocation points is applied in a prescribed manner, usually uniformly, to an entire arc of the boundary, and hence must be locally inappropriate at many points along that arc. The discretization of the boundary for this purpose is typically quite crude, and yet the method seems to resolve, quite successfully, comparatively small-scale variations along the wall. It is also typical of most applications of the method, that slip velocities below a certain threshold will be ignored. This prevents the generation of a host of very feeble vortex elements, which would add far more to the cost of the calculation than to the accuracy of its results.

2.6. *Stochastic Nature of the Results*

The results of a random-vortex calculation are intrinsically stochastic, so that analyses of accuracy and convergence of the method [36–40] produce estimates of the variance to be expected in a collection of statistically independent calculations. The cited analyses provide useful guidelines for some choices of computational parameters, but the flows to which they apply are all in some essential way simpler than the flow studied here. In particular, no analysis has yet been made of the convergence of a scheme in which vorticity is directly represented by sheets near the wall, and by blobs elsewhere, and no analysis contemplates the presence of a wall with sharp corners. Such complications will presumably receive attention within the next few years, and that will be a great help to users of the method.

The additional point to which attention is drawn here is that all analyses of convergence of the random vortex method implicitly assume stability of the flow being simulated. That is, they assume that the real flow will evolve nearly identically in each of a collection of realizations, distinguished from one another only by small, random, discrepancies in initial data. Thus, the variance which appears in a collection of numerical simulations is supposed to be a computational artifice, which can be reduced to a negligible level by refinement of computational parameters. However, real flows at sufficiently high Reynolds number are not stable in this sense, and it seems at least possible that the random displacements of vortex blobs, which necessarily change whenever the number of blobs or the time step is changed, might correspond to weak physical disturbances, sufficient to cause a large change in the subsequent evolution of a real flow. If this is true, the mean behavior of a collection of numerical simulations may not correspond to any single physical

realization of the flow, but to something akin to the ensemble-averaged behavior of a turbulent flow.

Analysis of the wall-driven cavity flow is complicated, in this respect, by the fact that nothing much is known about the stability of the flow. It has been difficult to ascertain, in this study, whether some unexpected development in the random-vortex simulation is a numerical aberration or a newly discovered physical instability. A very small ensemble, $N=3$, of calculations was carried out for each value of the Reynolds number, in the hope that some striking increase of variance would appear as Re increased. Nothing much was learned from this, possibly because the variance due to numerical discretization remained too large. However, the computational cost of refined random-vortex computations is fairly rapidly decreasing, and the idea of such a test for physical instability of complex flows may be worth another trial in the future.

3. Details of This Random-Vortex Calculation

3.1. *Convection Calculations*

The formula for the velocity induced by a line vortex within a stationary rectangle has appeared before in this journal [32]. It has been applied to the present task as follows:

(1) *Velocity induced on a blob.* Equations (1) and (2) below give the velocity components of a blob. For generality, the walls of the enclosure are the planes $x=0$ and $x=a$, $y=0$ and $y=b$. For our case, $a=b=1$.

$$
\begin{aligned}
u_i = {} & \frac{K\Gamma_i}{2\pi a} \frac{cn\left(\frac{2Ky_i}{a}, k'\right) dn\left(\frac{2Ky_i}{a}, k'\right)}{\left[1+cs^2\left(\frac{2Kx_i}{a}, k\right)+cs^2\left(\frac{2Ky_i}{a}, k'\right)\right] sn^3\left(\frac{2Ky_i}{a}, k'\right)} \\
& + \sum_{j\neq i} [p_y(x_i-x_j,\, y_i-y_j) + p_y(x_i-2a+x_j,\, y_i-2b+y_j) \\
& - p_y(x_i-x_j,\, y_i-2b+y_j) - p_y(x_i-2a+x_j,\, y_i-y_j)] \\
& + \sum_1 \left[\frac{\Gamma_j(y_i-y_j)}{2\pi|\mathbf{x}_i-\mathbf{x}_j|^2} - \frac{\Gamma_j(y_i-y_j)}{2\pi|\mathbf{x}_i-\mathbf{x}_j|\, r_0}\right] \\
& + \sum_2 \left[\frac{\Gamma_j(y_i-y_j')}{2\pi|\mathbf{x}_i-\mathbf{x}_j'|^2} - \frac{\Gamma_j(y_i-y_j')}{2\pi|\mathbf{x}_i-\mathbf{x}_j'|\, r_0}\right]
\end{aligned} \tag{1}
$$

$$
\begin{aligned}
v_i = & -\frac{K\Gamma_i}{2\pi a}\frac{cn\left(\frac{2Kx_i}{a}, k\right) dn\left(\frac{2Kx_i}{a}, k\right)}{\left[1+cs^2\left(\frac{2Kx_i}{a}, k\right)+cs^2\left(\frac{2Ky_i}{a}, k'\right)\right] sn^3\left(\frac{2Kx_i}{a}, k\right)} \\
& + \sum_{j\neq i}\left[-p_x(x_i-x_j,\, y_i-y_j) - p_x(x_i-2a+x_j,\, y_i-2b+y_j)\right. \\
& \left. + p_x(x_i-x_j,\, y_i-2b+y_j) + p_x(x_i-2a+x_j,\, y_i-y_j)\right] \\
& + \sum_{j\neq i}{}_1\left[-\frac{\Gamma_j(x_i-x_j)}{2\pi|\mathbf{x}_i-\mathbf{x}_j|^2}+\frac{\Gamma_j(x_i-x_j)}{2\pi|\mathbf{x}_i-\mathbf{x}_j|\, r_0}\right] \\
& + \sum{}_2\left[-\frac{\Gamma_j(x_i-x_j')}{2\pi|\mathbf{x}_i-\mathbf{x}_j'|^2}+\frac{\Gamma_j(x_i-x_j')}{2\pi|\mathbf{x}_i-\mathbf{x}_j'|\, r_0}\right],
\end{aligned} \tag{2}
$$

where

$$
K=\int_0^{\pi/2} d\varphi/(1-k^2\sin^2\varphi)^{1/2}, \qquad K'=\int_0^{\pi/2} d\varphi/(1-k'^2\sin^2\varphi)^{1/2} \tag{3}
$$

and

$$
p_x(x_i, y_i) = -\frac{K\Gamma_j}{2\pi a}\frac{cn^2\left(\frac{Ky_i}{a}, k'\right) cn\left(\frac{Kx_i}{a}, k\right) sn\left(\frac{Kx_i}{a}, k\right) dn\left(\frac{Kx_i}{a}, k\right)}{\left[1-cn^2\left(\frac{Kx_i}{a}, k\right) cn^2\left(\frac{Ky_i}{a}, k'\right)\right]} \tag{4}
$$

$$
p_y(x_i, y_i) = -\frac{K\Gamma_j}{2\pi a}\frac{cn^2\left(\frac{Kx_i}{a}, k\right) cn\left(\frac{Ky_i}{a}, k'\right) sn\left(\frac{Ky_i}{a}, k'\right) dn\left(\frac{Ky_i}{a}, k'\right)}{\left[1-cn^2\left(\frac{Kx_i}{a}, k\right) cn^2\left(\frac{Ky_i}{a}, k'\right)\right]}. \tag{5}
$$

The first term in (1) or (2), due to Greenhill [41], gives the effect of the blob's own image system, each image being treated as a line vortex.

The second group of terms adds the contributions of other blobs and their image systems, as though blobs and images were all line vortices.

The third group replaces the contribution of a line vortex by that of a blob, for each neighboring blob that lies within a distance r_0 (a blob radius) of the element of interest.

The fourth and last group replaces the contribution of a line vortex by that of a blob, for an image of any blob, if the image lies within a distance r_0 (a blob radius) of the element of interest. Note that this requires, for the first time, a calculation of the position of an image.

The functions p_x and p_y are defined by Eq. (4) and (5). In all of this: *cs* denotes the ratio *cn/sn*; Γ_i is the circulation of the blob whose velocity is being com-

puted—it multiplies Greenhill's expression for the effect of all the images of that blob; $\sum_1$ is taken over all values of $j \neq i$, such that the jth real blob overlaps the center of the ith blob; $\sum_2$ is taken over all values of j, such that an image of the jth real blob overlaps the center of the ith blob; k is the modulus of the elliptic integrals; $k' = (1-k^2)^{1/2}$; K and K' are the complete elliptic integrals corresponding to the moduli k and k'. The value of k is determined by the aspect ratio of the rectangular enclosure, by the relation $a/b = K/K'$. For a square, $k = k' = \arcsin(\pi/4)$ and $K = K' = 1.8541$. An iterative algorithm which exploits the descending Landen transformation [42] was used to evaluate the elliptic functions.

This direct mode of converting line vortices to blobs, when that would make a difference in the velocity of the element of interest, involves the subtraction of two large numbers to get a small difference. In principle, the difference can be obtained directly by a Taylor series expansion of the expressions involving elliptic integrals, for small values of the separation between elements. The appropriate formulas are, for the present case of a square enclosure,

$$p_x(x, y) \approx -\Gamma_j(x/2\pi r^2) + K^2\Gamma_j(x/24\pi a^2) \times \{(10-8\sqrt{2})\sin^4\theta - 2\sin^2\theta + (9+4\sqrt{2})\} \tag{6}$$

and

$$p_y(x, y) \approx -\Gamma_j(y/2\pi r^2) + K^2\Gamma_j(y/24\pi a^2) \times \{(10-8\sqrt{2})\cos^4\theta - 2\cos^2\theta + (9+4\sqrt{2})\}. \tag{7}$$

In these formulas, $x = x_i - x_j$, $y = y_i - y_j$, $r^2 = x^2 + y^2$, $\sin^2\theta = y^2/r^2$, and $\cos^2\theta = x^2/r^2$. These expressions are accurate to about one part in 10^8 if $r \leqslant 10^{-4}$. When $r < r_0$, we have only to set $r = r_0$ in the leading terms. This analysis, suggested by the work of Sherman [43], was unfortunately done too late to help with the present calculations, for which a truncated summation of image effects, using 1200 nearest images, was used if r was $\leqslant 10^{-4}$.

(2) *Velocity induced on a sheet.* The velocity induced at the midpoint of a sheet includes the contributions of blobs, just described above, plus the contributions of any sheets that shadow the sheet of interest. Formulas for the latter contributions, accounting for partial shadowing, have been given by Chorin [29] and were used unchanged.

3.2. *Location of the Points of Zero Slip*

Each wall, of dimensionless length unity, was divided into equal segments of dimensionless length h; the no-slip condition was enforced at the midpoint of each segment.

After some trial runs with $h = 0.2$ (too coarse), and $h = 0.05$ (too expensive), we compromised on $h = 0.1$. (All such choices of discretization parameters are summarized in Table I.)

TABLE I

Parameters of the Random-Vortex Computations

R	2000	5000	10.000
r_0	$0.1/\pi$	$0.1/\pi$	$0.1/\pi$
h	0.1	0.1	0.1
$u_{\min}$	0.125	0.125	0.125
Δt	0.2	0.2	0.1
$t_{\max}$	3	3	2
Ensemble size	3	3	3

3.3. *Thickness of Sheet Layer*

The thickness of the sheet layer is constrained by two considerations:

(1) If it is less than half a blob radius, then a blob and its nearest image induce the same tangential velocity at the wall, as would a sheet and its image, providing that blob and sheet have equal circulation and that $h = \pi r_0$. Here h is the sheet length and r_0 is the blob radius [29]. This would be true even if the layer were twice as thick, but the constraint given here also implies that the velocity induced on the interior element by its image is independent of element status.

(2) It is a nuisance to have blobs randomly walking through the wall, and this can be avoided by letting the sheet-layer thickness exceed about 2σ, where σ is the standard deviation of the distribution of random steps.

Since the value of σ depends on the size of the time step, these two constraints jointly imply a constraint on Δt. Specifically, if the sheet-layer thickness, δ, is set equal to $n\sigma$, the constraint is $\Delta t \leqslant h^2 R/8\pi n^2$. (In this, and in all subsequent citations of numerical values, the unit of time is L/U and the Reynolds number is $R = UL/\nu$, where U and L are the sliding wall velocity and length, respectively; L/U, U and L are used for nondimensionalization.) We have chosen $n = 2$ and $h = 0.1$, and will present calculations for $R = 2000$, 5000, and 10.000. Thus any value of $\Delta t \leqslant 0.2$ would meet these constraints.

3.4. *Circulation of Vortex Elements; Maximum Tolerable Slip Velocity*

As was mentioned in Section 2.5, no effort is made to annihilate the slip velocity exactly at a given collocation point. To cancel $\mathbf{u}_{\text{slip}}$ approximately, N sheets of the appropriate sign, each causing a velocity jump $u_{\min}$, are generated. N is the integer part of $|\mathbf{u}_{\text{slip}}|/\mathbf{u}_{min}$, so the maximum residual slip velocity is u_{min}. The circulation of the resulting vortex elements is thus $\Gamma = hu_{\min}$.

In the experience of most users of the random-vortex method, $u_{\min}$ is the parameter to which the behavior of the simulation is most sensitive. We picked the largest value for which the oscillations associated with parasitic vortex elements were not serious. This was the value $u_{\min} = 0.125$.

3.5. *Time Step*

The value of the time step affects both the accuracy of the convection calculation and the prominence of the stochastic aspects of the simulation. We used $\Delta t = 0.1$ for $R = 10.000$. In this choice, as in all others, we picked discretization levels that kept the calculation as inexpensive as possible while yielding results free of any obviously nonphysical features. We do not claim that these results are quantitatively independent of further refinement of the discretization. They were achieved with a number of vortex elements which started off at about 80, and rose to about 300 at time $t = 3$. This seems like a very small number of elements, but they were all crowded into about one-fifth of the total area of the square, and suffice to show events there with fair detail.

3.6. *Ensemble Calculations*

To obtain some idea of the variance of the results and to obtain averaged values for comparison with finite-difference calculations and experiment, each random-vortex calculation was run three times, with identical parameters but with different points of entry to the computer's string of random numbers.

3.7. *Treatment of Random Displacements That Cross a Wall*

The random displacement of a sheet often carries it out of the cavity, and the same is occasionally true of blobs. These events were treated in the way prescribed by Chorin [29], where the rational is given. Specifically:

(1) A sheet that moves a distance y beyond the wall is replaced in the fluid, at a distance y from the wall. If $y > \delta$, the sheet is then converted to a blob.

(2) A blob that moves a distance y beyond the wall is discarded if $y > \delta$; otherwise it is converted to a sheet and then replaced in the fluid, at a distance y from the wall.

3.8. *Special Treatment of Corner Regions*

Each corner region was accorded special treatment, as is shown in Fig. 2.

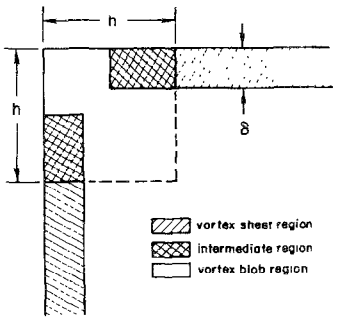

FIG 2. Showing the way that corner regions in the enclosure are modeled using vortex sheets, vortex blobs, and a combination of the two. δ is shown approximately to scale for $\Delta t = 0.2$, $R = 2000$.

Whenever a vortex element is found in the clear region of the sketch, it is treated as a blob; in the singly-hatched regions it is treated as a sheet; in the doubly-hatched region, its effect on a blob is that of another blob, while its effect on a sheet is that of another sheet. When a blob is close to a wall, and especially to a corner, a test is made of its proximity to each of the three nearest image blobs. Whenever one of the image blobs overlaps the real blob its contribution to the velocity of the real blob is modified, by subtracting off the effect of a line vortex and adding back the effect of a blob (just as though the image blob were a sufficiently nearby real blob).

There may be more elegant ways to treat corners, but it is recognized that the corners where stationary walls abut the moving wall are not like ordinary interior corners, where two stationary walls meet and there is a stagnation point. One presumes that all numerical treatments of this problem must avoid any reference to the velocity precisely at the corners by the moving wall.

3.9. *Computational Costs and Their Distribution*

Computations employing the Biot–Savart integral in a straightforward way are notorious for rapid growth of the number of operations, as the number of vorticity elements is increased. If no clever grouping strategy is used, the count grows as the square of the number of elements, and it does so in our case.

The number of operations required for each element depends on the kind of element and on the technique used to compute $\mathbf{u}_p$. Each element is affected by every blob and by a relatively few (perhaps five) sheets. In turn, each blob affects every other element, but a sheet affects only those few sheets that are in its shadow. The proportion of blobs to sheets increases as the calculation progresses, as shown in Fig. 3.

When an image method is used to compute $\mathbf{u}_p$, as was done in this work and the work of Cheer [20], Ghoniem *et al.* [35], and Ellzey [18], the number of operations required to compute the effect of one blob and its image system on any other element depends on the complexity of the image system. In the present case,

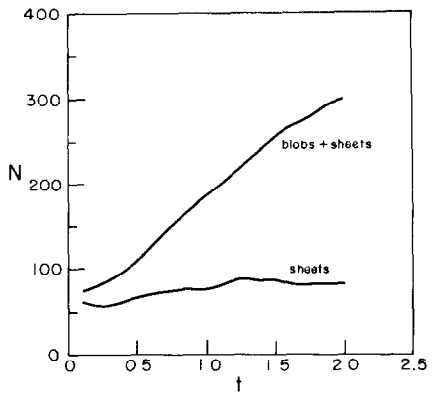

FIG. 3. Variation of the vortex elements with respect to time for $R = 10.000$.

the image system is very complex; the necessary computations require evaluation of the formulas (4) and (5). By the methods we used to evaluate the elliptic functions, the computation of the effect of one blob and its image system requires approximately 17 times the CPU time required to evaluate the corresponding formulas for a vortex blob in free space.

The principal alternative to the image system for the evaluation of $\mathbf{u}_p$ employs a fixed array of external singularities, as has been mentioned above, in Section 2.3. This is admittedly less accurate, but consumes an almost negligible fraction of the computational resources, thus allowing the use of a greater number of vortex elements within a fixed computing budget. The overall effect on accuracy of a field of $\mathbf{u}_p$ which is generated by any fixed array of external singularities may be an unacceptably strong function of time, because singularities which are arranged to do a good job once the vorticity is fairly well spread through the interior may allow unacceptable leaks through the wall at early times, when the vorticity is packed tightly along the belt and in one corner. Further investigation of this issue may well be useful. It might be possible to design a compromise scheme, in which the effect of the three nearest images of a blob near a corner is explicitly calculated, and a fixed array of external singularities is tuned to minimize the residual leakage.

4. The REBUFFS Code

The REBUFFS code has been previously described by LeQuere, Humphrey, and Sherman [22]. It has been used extensively to predict laminar and turbulent flows in enclosures and cavities [22–26]. Suffice it to say that the numerical algorithm as employed here uses second-order central differencing for diffusion terms and third-order quadratic upstream interpolation for convection [44], thus yielding a procedure that is second-order accurate globally; the algorithm is implicit and first-order accurate in time; within a time step the continuity and momentum equations are solved iteratively, until a pre-established convergence criterion is attained; between iterations the SIMPLE method of [45] is employed to correct and update the velocity and pressure fields on a staggered interconnected grid; within an iteration the flow domain is swept line-by-line and the difference equations along a line solved using the Thomas algorithm. With respect to the quadratic upstream interpolation technique, the improved procedure developed by Freitas *et al.* [24] was implemented, which guarantees diagonal dominance of the coefficients in the inversion matrix at all times for constant density flows.

Additional checks and validations of REBUFFS were performed and are reported in [46]. In particular, steady state calculations of the wall-driven enclosure flow at $R = 3200$ on 30×30 and 52×52 non-uniform grids showed very good agreement with the superrefined grid calculations of [10].

5. Results and Discussion

In this section we first present and discuss calculations of the wall-driven enclosure flow using the REBUFFS code. The initial flow development was predicted for $R = 2000$ and 5000, respectively. These results provide the basis for a comparison with the random-vortex calculations performed for $R = 2000$, 5000, and 10.000. However, the comparison must be made cautiously, since the finite difference equations solved by REBUFFS yield results that are smoothed out in time and space by the discretization scheme and the finite grid. Therefore, perturbations tend to be damped out. By contrast, a vortex method solution provides a more realistic picture of the flow, in that it yields a sequence of possible instantaneous realizations as a function of time (subject to constraints related to the finite number of vortex elements, their finite dimensions, and the finite calculation time step).

To make a meaningful comparison between the two procedures at any time, t, the mean flow characteristics derived from an ensemble of vortex method solutions should be obtained. Because a large ensemble is prohibitively expensive to generate, we are limited to averages of three independent solutions with identical flow conditions excepting the initial seed of random number generation (say initial seed $I = 5$, 10, 15) to obtain a smoothed solution at time t. Clearly, particularly during the early stages of flow development, such a procedure is bound to be coarse. Nevertheless, it has been dictated by practical considerations. Although limited, the availability of experimental data [1] at $R = 2000$ broadens the basis for a comparative evaluation.

Space limitations make it necessary to focus on the principal findings of this study. For this we have chosen representative samples of the large volume of numerical data available. The reader is referred to Choi [46] for a complete record of the calculations.

5.1. *REBUFFS Calculations*

These calculations were performed on a non-uniform (30×30) grid after it had been determined that further refinement affected the results only marginally. A time step of $\Delta t = 0.2$ was used for both values of the Reynolds number ($R = 2000$ and 5000).

The calculation for $R = 2000$ was conducted to steady state. The developed solution of the flow is shown in Fig. 4, where the length of a vector is proportional to the speed of the fluid at the base of the vector, and the arrow indicates the local direction of the flow. The principal characteristics of the developed flow solution are the presence of: one large clockwise-rotating eddy in the center of the enclosure; one counterclockwise rotating secondary eddy in each of three of the enclosure corners; and, one clockwise-rotating tertiary eddy in the bottom right-hand corner of the enclosure. (The tertiary eddy is hard to see in the figure, but is defined by the four vectors most closely located to this corner.) This solution, including the prediction of the tertiary eddy, is in good agreement with the results given in [10].

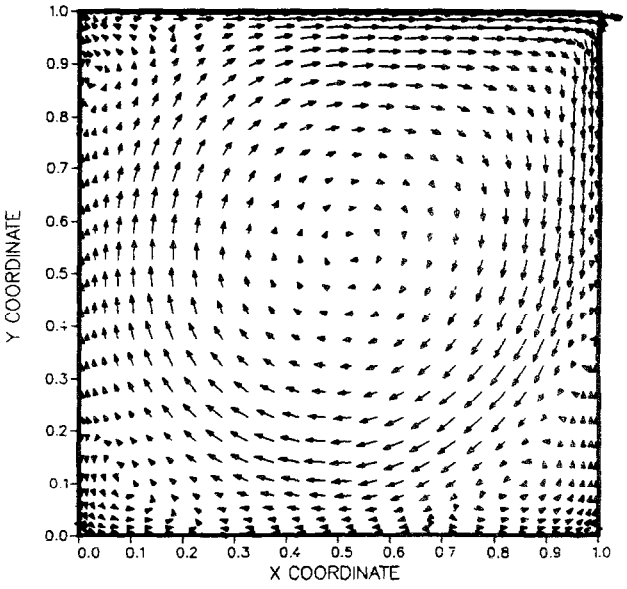

FIG. 4. Velocity vector plot showing REBUFFS calculations of developed, steady state, wall-driven enclosure flow at $R = 2000$.

As the enclosure flow develops (a detailed sequence of vector plots is given in [46]) the center of rotation of the main eddy is displaced from the top right-hand corner of the enclosure towards its center. The first of the secondary eddies

side of the enclosure at $t \simeq 6$, and between $t = 6$ and 13 it grows very little. However, by the time steady state is achieved its size has increased considerably. The times of the appearance of the third secondary eddy (in the top left-hand corner of the enclosure) and the tertiary eddy were not determined.

The initial developments of the flows at $R = 2000$ and 5000 are very similar. However, at $R = 5000$ an interesting detail appears more clearly. This is shown in the sequence of plots in Fig. 5. At $t = 2$ a secondary eddy appears along the side wall of the enclosure beneath the main eddy generated by the moving wall. Its coordinates are $x = 0.99$ and $y = 0.69$ approximately. As time increases this secondary eddy is displaced vertically downwards. However, its vorticity is diffused before it has a chance to reach the bottom right-hand corner of the enclosure. Therefore, it does not appear to be the cause for the secondary eddy that appears subsequently at this location. Using flow visualization, Sinha [47] has observed the presence of the above secondary side-wall eddy during the very initial stages of flow development in his enclosure. More will be said about this interesting structure in relation to the random-vortex calculations.

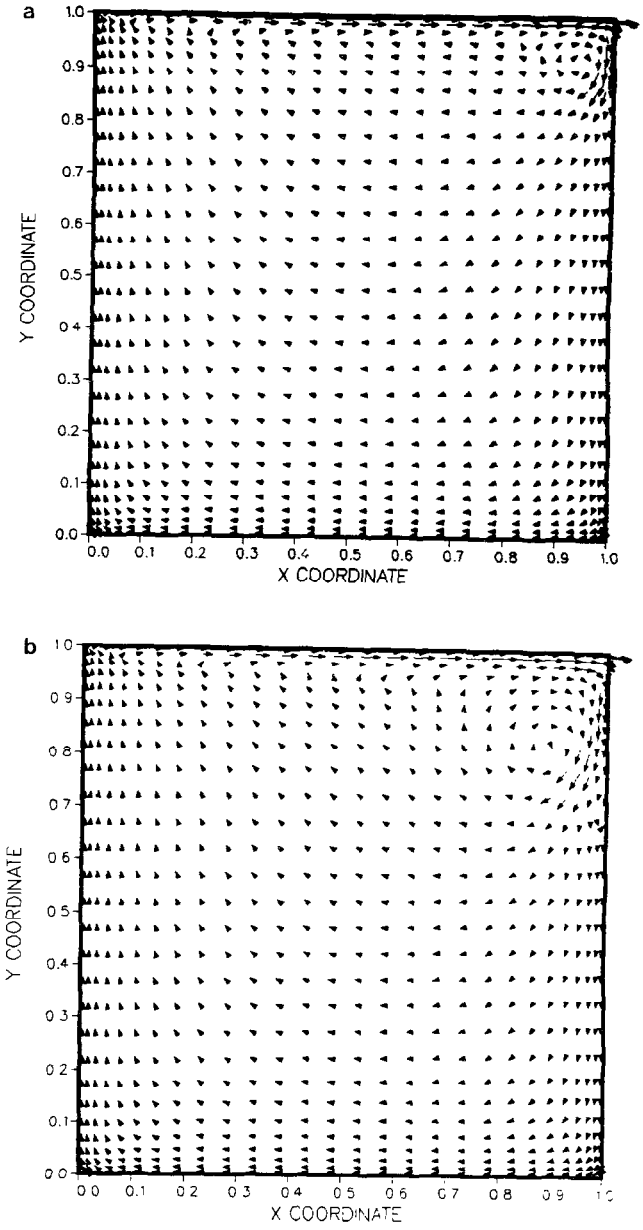

FIG. 5. Velocity vector plots showing REBUFFS calculations of developing wall-driven enclosure flow at $R = 5000$; $t = 1$, 2, and 3 in Figs. a, b, and c, respectively.

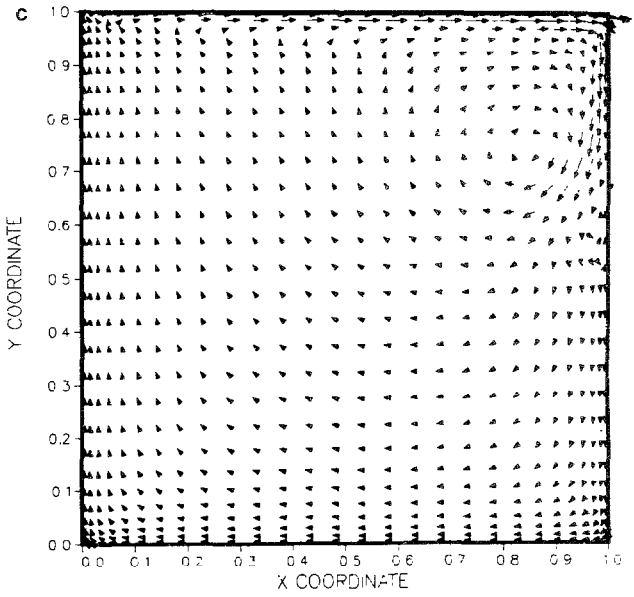

FIG. 5—*Continued.*

5.2. *Random-Vortex Calculations*

The random-vortex method was used to predict the wall-driven enclosure flow at $R = 2000$, 5000, and 10.000. In all cases the start-up flow displayed evolving vortical structures along the moving wall of the enclosure. As the flow evolved these structures were convected towards the downstream corner of the moving wall, where the main recirculating flow in the enclosure evolves. In all major respects the characteristics of the flows at $R = 2000$ and 5000 were the same; see [46].

Figures 6 and 7 show instantaneous vortex element velocity vectors and streamline contour plots of the flow at $R = 2000$ for $t = 2$ and 3, respectively. The appearance of the secondary eddy below the main recirculation zone is quite striking at $t = 3$. The streamline plots show the extent to which the main recirculating flow evolves in the enclosure. Between $t = 2$ and 3, the center of the main eddy has been significantly displaced toward the enclosure center.

Figure 8 is a velocity vector plot of the flow, derived from the vorticity field, for $R = 10.000$ at $t = 2$. The most striking feature in the plot is the *ejection* of the small secondary eddy from the vertical sidewall toward the enclosure center by the main corner eddy. Such an ejection did not appear in the lower Reynolds number calculations of the flow.

The repetition of random-vortex calculations using different initial seed values allowed the determination of mean velocity profiles from samples of 3 calculations. The results for $R = 2000$ are shown in Fig. 9a and 10a for different locations in the enclosure. Corresponding results calculated with the REBUFFS code are shown in

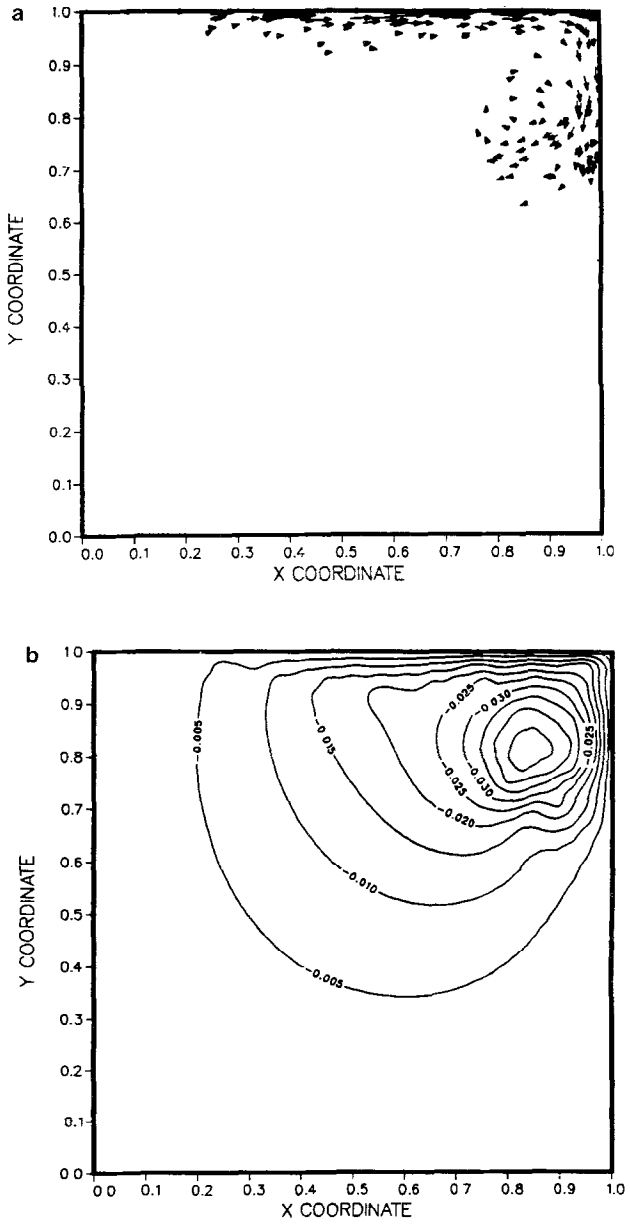

FIG. 6. (a) Instantaneous vortex element positions and velocities at those positions: $R = 2000$, $t = 2$; (b) streamline contours plot corresponding to Fig. 6a.

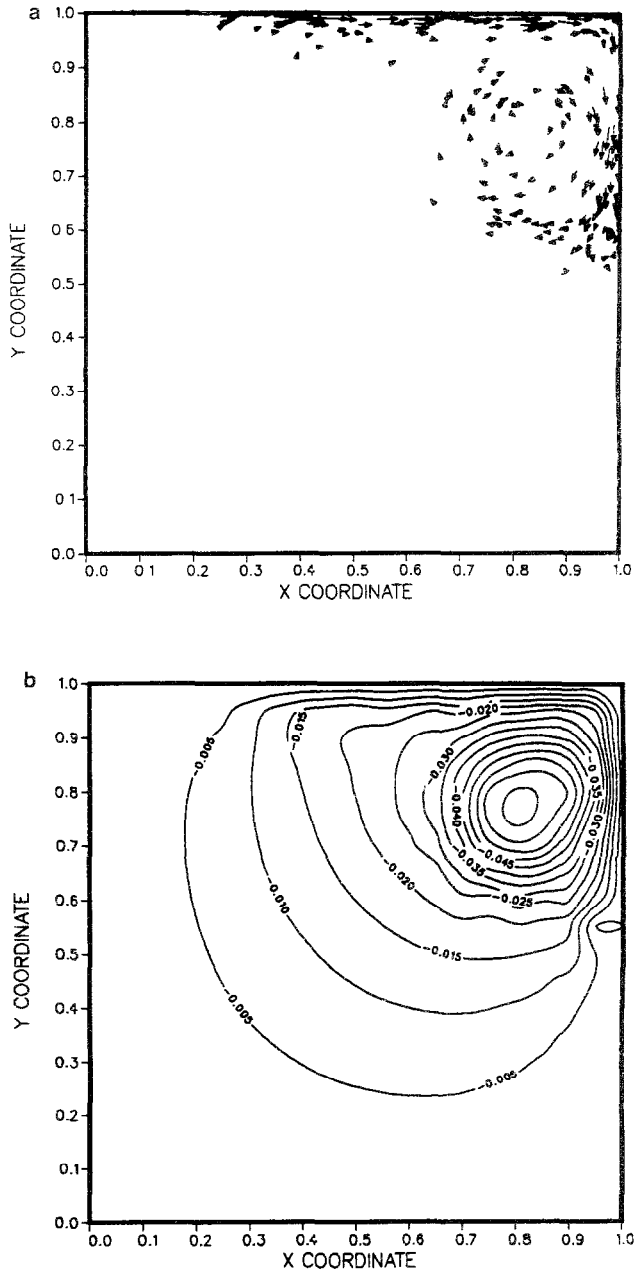

FIG. 7. (a) Instantaneous vortex element positions and velocities at those positions: $R = 2000$, $t = 3$; (b) streamline contours plot corresponding to Fig. 7a.

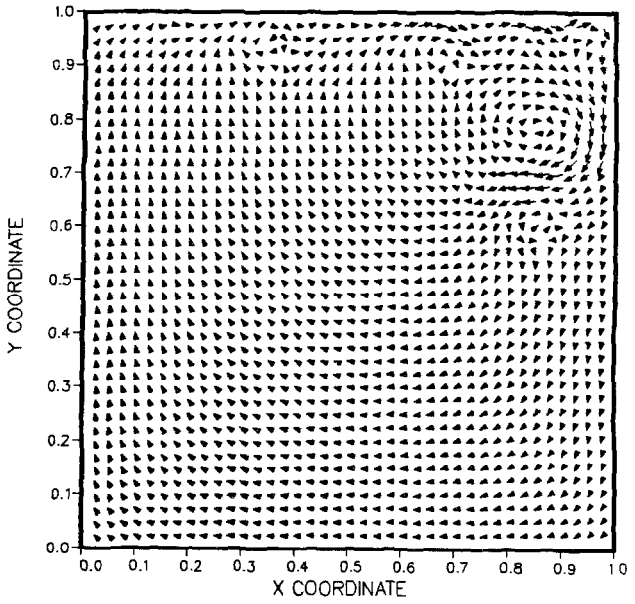

FIG. 8. Velocity vector plot derived from random vortex method calculations: $R = 10.000$, $t = 2.0$.

Figs. 9b and 10b. The agreement between the two sets of results is fairly good. Similar agreement was obtained for the calculations at $R = 5000$; see [46].

Calculated locations of the main recirculating flow center are shown in Fig. 11, as a function of time, for the three Reynolds numbers investigated. For $R = 10.000$ only vortex method results are available. For $R = 5000$ agreement is good between the vortex method calculations and results obtained using the REBUFFS code. For $R = 2000$, the random-vortex scheme results are in slightly better agreement with the measurements than the REBUFFS calculations.

6. CONCLUSIONS

The initial unsteady wall-driven flow in a 2D rectangular enclosure at high Reynolds number was simulated using the random-vortex scheme. Vortex sheets were employed in boundary layer regions near walls, while blobs were used in the core of the flow and in corners. A closed form solution in terms of elliptic functions was used as the basis to compute the velocity field induced by the vortex blobs in the enclosure. A special treatment of flow regions near the enclosure corners, where the use of sheet-elements is inappropriate, was necessary. This has consisted in defining a short transition region between each corner (where only blobs are used) and the two boundary layers at right angles adjacent to it (where only sheets are

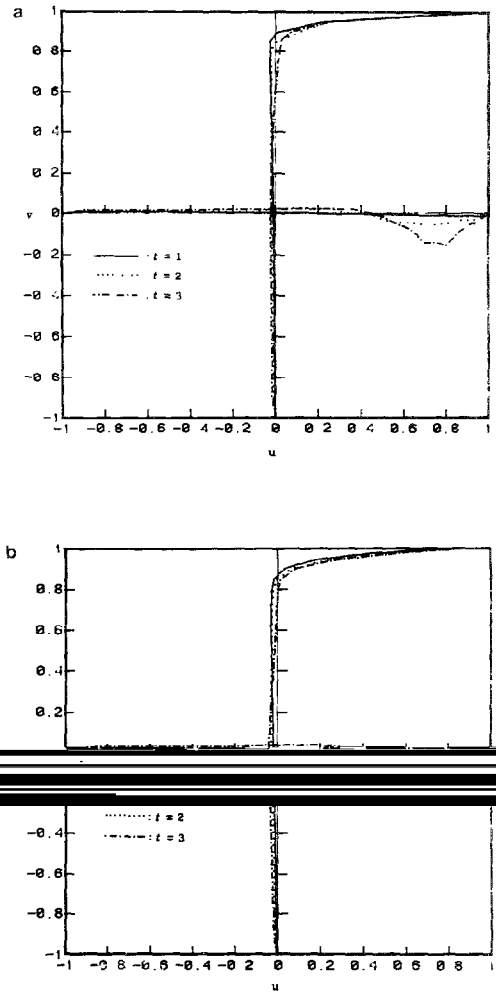

FIG. 9. (a) Random vortex method calculations of the average velocity profiles at the symmetry planes for $R = 2000$: (b) REBUFFS code calculations of the velocity profiles at the symmetry planes for $R = 2000$.

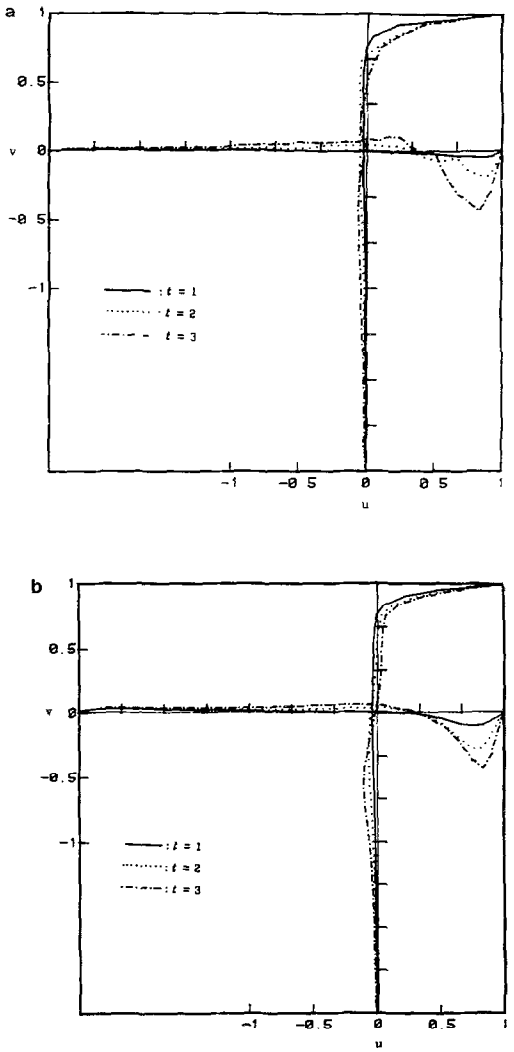

FIG. 10. (a) Random vortex method calculations of the average velocity profiles at two planes near the main vortex center for $R = 2000$; (b) REBUFFS code calculations of the velocity profiles at two planes near the main vortex center for $R = 2000$.

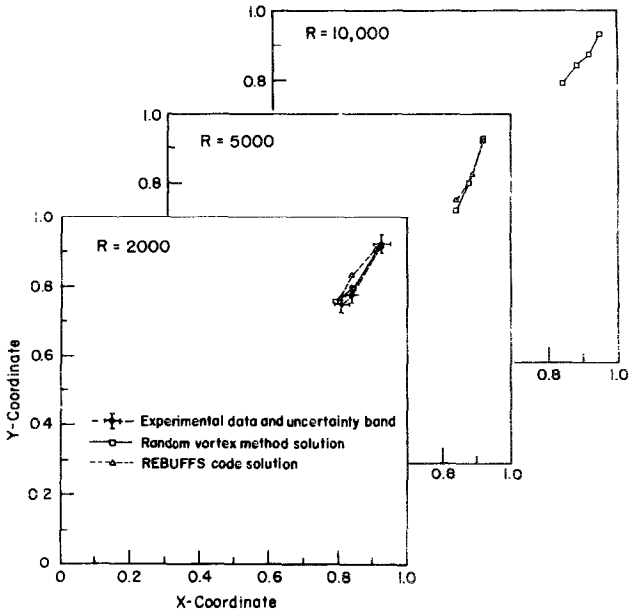

FIG. 11. Relative comparison of calculated main vortex core location; points for $R = 2000$ and 5000 are plotted at values $\Delta t = 1.0$ apart. Points for $R = 5000$ are $\Delta t = 0.5$ apart. The experimental values at $t = 3$ were obtained by interpolating data at $t = 2$ and 4 in [1].

used), in which the effect of a vortex element on a blob is as if it were another blob, while its effect on a sheet is as if it were another sheet.

The calculations accurately reveal the growth of the main vortex that originates in the corner downstream of the sliding wall, as well as the presence of transient secondary flow structures that are due to the convection and diffusion of vorticity from this region of the flow. The distribution and intensities of the secondary structures depend strongly on Reynolds number. How they ultimately evolve with time is a matter for further research.

Comparisons between the random-vortex calculations and the limited experimental data available show good agreement. Good qualitative agreement is also obtained with respect to calculations obtained using a transient finite difference procedure.

ACKNOWLEDGMENTS

This study was supported in part by the Department of Energy, Office of Basic Energy Sciences, through Grant DE-GF-85ER13397. The authors gratefully acknowledge the encouragement and helpful suggestions provided by Professor A. Chorin and Professor A. Ghoniem. We are indebted to Dr. W. M. To for his assistance in adapting the REBUFFS code to the present problem. Thanks are due to Sue Bavonese for the typing of this manuscript. The authors' names are listed in alphabetical order.

REFERENCES

1. J. R. KOSEFF, "Momentum Transfer in a Complex Recirculating Flow," Ph.D. thesis. Stanford University, 1983 (unpublished).
2. R. D. MILLS, *J. R. Aeronaut. Soc.* **69**, 116 (1965).
3. O. BURGGRAF, *J. Fluid Mech.* **24**, 113 (1966).
4. J. D. BOZEMAN AND C. DALTON, *J. Comput. Phys.* **12**, 348 (1973).
5. A. G. HUTTON, in *Proceedings, Third International Conference on Finite Elements in Fluid Problems, Banff, Alberta*, 1980, p. 10.
6. R. PIVA, A. DI CARLO, AND G. GUJ, *Comput. Fluids* **8**, 225 (1980).
7. J. C. HEINRICH, AND R. S. MARSHALL, *Comput. Fluids* **9**, 73 (1981).
8. S. G. RUBIN, AND P. K. KHOSLA, *Comput. Fluids* **9**, 163 (1981).
9. R. K. AGARWAL, "A Third-Order-Accurate Upwind Scheme for Navier-Stokes Solutions at High Reynolds Numbers," AIAA 19th Aerospace Sciences Meeting, St. Louis, January 12, 1981.
10. U. GHIA, K. N. GHIA, AND C. T. SHIN, "Solution of Incompressible Navier-Stokes Equations by Coupled Strongly Implicit Multigrid Methods," Symposium on Multigrid Methods, NASA-AMES Research Center, Moffett Field, CA, October 21, 1981.
11. R. SCHREIBER, AND H. B. KELLER, *J. Comput. Phys.* **49**, 310 (1983).
12. A. M. GOORAY, C. B. WATKINS, AND W. AUNG, in *Proceedings of the Joint Conference on Thermal Engineering*. ASME-JSME, Honolulu, Hawaii, March 20, 1983 p. 79.
13. A. D. GOSMAN, W. M. PUN, A. K. RUNCHAL, D. B. SPALDING, AND M. WOLFSHTEIN, *Heat Transfer in Recirculating Flows*, (Academic Press, London, 1969).
14. F. J. K. IDERIAH, in *Proceedings of First International Conference on Numerical Methods in Laminar/Turbulent Flow*, 1978, p. 257.
15. T. HAN, J. A. C. HUMPHREY, AND B. E. LAUNDER, *Comput. Meths. Appl. Mech. Eng.* **29**, 81 (1981).
16. D. L. YOUNG, J. A. LIGETT, AND R. H. GALLAGHER, *J. Eng. Mech. Div. Amer. Soc. Civ. Eng.* **102, EM1**, 1 (1976).
17. A. N. FINDIKAKIS AND R. L. STREET. *J. Hydraul. Div. Amer. Soc. Civ. Eng.* **108, HY8**, 904 (1982).
18. J. L. ELLZEY, "Experimental and Numerical Study of a Two-Stream, Planar, Turbulent Mixing Layer," Ph.D. thesis, Univ. of California, Berkeley, 1985 (unpublished).
19. A. F. GHONIEM AND Y. GAGNON, *J. Comput. Phys.* **68**, 346 (1986).
20. A. Y. CHEER, "Numerical Analysis of Time Dependent Flow Structure Generated by an Impulsively Started Circular Cylinder in a Slightly Viscous Incompressible Liquid," Center for Pure and Applied Mathematics Report PAM-145, Univ. of California, Berkeley, 1983 (unpublished).
21. E. C. TIEMROTH, "Simulation of the Viscous Flow around a Cylinder by the Random-Vortex Method," Ph.D. thesis, Univ. of California, Berkeley, 1986 (unpublished).
22. P. LEQUERE, J. A. C. HUMPHREY, AND F. S. SHERMAN, *Numer. Heat Transfer* **4**, 249 (1981).
23. J. R. KOSEFF, R. L. STREET, P. M. GRESHO, C. D. UPSON, J. A. C. HUMPHREY, AND W. M. TO, in *Proceedings, Third International Conference on Numerical Methods in Laminar/Turbulent Flow, Seattle, WA, August* 1983.
24. C. J. FREITAS, R. L. STREET, A. N. FINDIKAKIS, AND J. R. KOSEFF, *Int. J. Numer. Methods Fluids* **5**, 561 (1985).
25. W. M. TO AND J. A. C. HUMPHREY, *Int. J. Heat Mass Transfer* **29**, 573 (1986).
26. J. A. C. HUMPHREY, AND W. M. TO, *Int. J. Heat Mass Transfer* **29**, 593 (1986).
27. A. J. CHORIN, *J. Fluid Mech.* **57**, 785 (1973).
28. A. J. CHORIN, *J. Comput. Phys.* **27**, 423 (1978).
29. A. J. CHORIN, *SIAM J. Sci. Statist. Comput.* **1**, 1 (1980).
30. J. T. BEALE, AND A. MAJDA, *J. Comput. Phys.* **58**, 188 (1985).
31. M. PERLMAN, *J. Comput. Phys.* **59**, 200 (1985).
32. Y. CHOI, AND J. A. C. HUMPHREY, *J. Comput. Phys.* **56**, 15 (1984).
33. B. CARNAHAN, H. A. LUTHER, AND J. O. WILKES, *Applied Numerical Methods*, (Wiley, New York, 1969).

34. O. H. HALD, *SIAM J. Sci. Statist. Comput.* **2**, 85 (1981).
35. A. F. GHONIEM, A. J. CHORIN, AND A. K. OPPENHEIM, *Philos. Trans. R. Soc. London A* **304**, 303 (1982).
36. O. H. HALD, *SIAM J. Sci. Statist. Comput.* **7**, 1373 (1986).
37. S. G. ROBERTS, "Convergence of a Random-Walk Method for the Burgers Equation," Center for Pure and Applied Math, University of California, Berkeley, CA, PAM-305, October 1985 (unpublished).
38. G MARCHIORO AND M. PULVIRENTI, "Vortex Methods in Two-Dimensional Fluid Mechanics," Lecture Notes in Physics Vol. 206 (Springer-Verlag, New York, 1985).
39. G. BENFATTO AND M. PULVIRENTI, Convergence of Chorin's product formula in the half-plane, *Commun. Math. Phys.*, in press.
40. D.-G. LONG, "Convergence of the Random Vortex Method in One and Two Dimensions," Ph.D. dissertation, Dept. of Mathematics, Univ. of California, Berkeley, 1986 (unpublished).
41. A. G. GREENHILL, *Q. J. Math.* **15**, 24 (1878).
42. M. ABRAMOWITZ AND I. A. STEGUN, *Handbook of Mathematical Functions*, (Dover, New York, 1970), p. 573.
43. F. S. SHERMAN, "Convective Enhancement of the Potential for Molecular Mixing. A case study: Kelvin–Helmholtz Waves." presented at INTAM Conference on Mixing in Stratified Fluids, Margaret River, Australia, 1985 (unpublished).
44. B. P. LEONARD, *Comput. Methods Appl. Mech. Eng.* **19**, 59 (1979).
45. S. V. PATANKAR, *Numerical Heat Transfer and Fluid Flow* (Hemisphere, New York, 1980).
46. Y. CHOI, "A Hybrid Random Vortex Method for Predicting Developing Two-Dimensional Wall Driven Flows in Rectangular Enclosures," Ph.D. thesis, Univ. of California, Berkeley, 1986.
47. S. K. SINHA, "An experimental Investigation of Recirculation and Destratification in Lid-Driven Cavity flows," Ph.D. thesis, University of Miami, 1986.